Beamforming-based wavepacket model for noise predictions of tactical aircraft

Tyce Olaveson, Blaine M. Harker and Kent L. Gee

Citation: Proc. Mtgs. Acoust. **29**, 040011 (2016); doi: 10.1121/2.0001639
View online: https://doi.org/10.1121/2.0001639
View Table of Contents: https://asa.scitation.org/toc/pma/29/1
Published by the Acoustical Society of America

Proceedings of Meetings on Acoustics

Volume 29 http://acousticalsociety.org/

172nd Meeting of the Acoustical Society of America

Honolulu, Hawaii

28 November to 2 December 2016

Noise: Paper 2pPA7

Beamforming-based wavepacket model for noise predictions of tactical aircraft

Tyce Olaveson
Department of Physics and Astronomy, Brigham Young University, Provo, UT, 84602; tyceolaveson@gmail.com;

Blaine M. Harker
Blue Ridge Research and Consulting LLC, Ashville, NC; Blaine.Harker@blueridgeresearch.com

Kent L. Gee
Department of Physics and Astronomy, Brigham Young University, Provo, UT, 84602; kentgee@byu.edu

Wavepacket models provide a convenient representation of jet noise source phenomena because of the extended, partially correlated nature of the turbulent mixing noise. When treated as an equivalent source model, they are useful to estimate features of both the radiated noise as well as the source characteristics to assist in jet noise reduction efforts. In this study, the hybrid beamforming method is applied to measurements in the vicinity of a high-performance military aircraft. These results are then decomposed into an azimuthally-averaged multi-wavepacket representation of the data, which can then be treated as an equivalent source. Estimates of the field levels and coherence properties using the equivalent source are compared with measurements, and results from the multi-wavepacket model show good agreement with benchmark measurements over a range of frequencies that contribute significantly to the overall radiation. The capabilities and limitations of the model to estimate field properties are quantified with respect to benchmark measurements in the mid and far fields as a function of frequency. Results indicate that the multi-wavepacket representation is an improvement over single-wavepacket models, which do not incorporate spatiotemporal features of the radiation.

Published by the Acoustical Society of America

 https://doi.org/10.1121/2.0001639

1. INTRODUCTION

This paper is an abridgment of chapter five of Dr. Harker's Ph. D dissertation Ref. [1]. The goal is to introduce the concept of wavepackets and their application to jet noise. While substantial information is provided here, the avid reader is directed to the dissertation for an in-depth exploration of wavepackets and the other methods (i.e., Hybrid Beamforming) referenced herein.

A. BACKGROUND

Wavepacket models provide a reduced-order, analytical and physical framework for describing acoustic, hydrodynamic, and turbulence-related features of jet noise.[2] They are defined as advecting disturbances that are correlated over distances exceeding the integral scales of turbulence and have been used to describe the Mach wave radiation of supersonic jet noise[2, 3] as well as subsonic noise.[4] Many studies have focused modeling the turbulent wavepackets to describe the jet physical behavior.[2-7] However, because of the harsh environment and hot, fast flows in the vicinity of full-scale jet noise measurements, the jet acoustic wavepacket properties are most easily analyzed using pressure measurements of the radiated field. Additionally, Towne *et al.*[8] found that the dominant turbulence wavepackets and those of the acoustic radiation were nearly uncorrelated. Acoustic phased array methods, such as beamforming, can be used to estimate equivalent wavepacket descriptions of the source, which can predict the radiation in terms of level and coherence, without the need to measure the source directly. [9-11]

B. EQUIVALENT ACOUSTIC WAVEPACKET MODELS IN JET NOISE STUDIES

Although not numerous, there are studies that provide context for acoustically modeling jet noise using wavepackets. Suzuki and Colonius[12] modeled the instability waves of near-field subsonic jet noise using an eigenfunction approach to beamforming. Kœnig *et al.*[4] decomposed far-field noise measurements of a subsonic cold laboratory jet using an orthogonal decomposition of the pressure field into a single modal component, which they compared to the radiation of a wavepacket model. Papamoschou[3] showed that one wavepacket per frequency could adequately describe the measured far-field levels for lower frequencies and in the peak radiation direction. Du and Morris[13] applied conventional beamforming to simulated far-field jet noise data to obtain the acoustic complex pressure at the jet lipline, which was then decomposed using a wavepacket model for Strouhal numbers of 0.3 and 0.6. When compared to the simulated far-field pressure measurements, the estimated pressure field from the first wavepacket mode showed general agreement. Reba *et al.*[14] measured the hydrodynamic pressure field and fit the amplitude and correlation measurements to Gaussian-shaped wavepackets of the first two azimuthal modes. When used to predict acoustic levels, each wavepacket model showed good agreement with acoustic measurements in the peak radiation region. Cavalieri *et al.*[15] found that the axisymmetric acoustic wavepacket of a subsonic lab-scale jet is more strongly coupled to the jet velocity than higher-order azimuthal acoustic wavepackets. They predicted the source size to be 6-8 diameters (D) in length and developed a model of the high-angle (measured relative to the jet inlet) downstream radiation. Additional work by Maia *et al.*[16] incorporated wavepacket self-coherence in a subsonic lab-scale jet study and showed that educed wavepackets of particle image velocimetry measurements that included coherence decay more accurately estimated the radiated levels. They also found that a decomposition of the modeled radiated levels indicated roughly ten modes were required to capture the top 10 dB of the radiated energy. These studies have shown that levels of the sound field have been shown to be reasonably reproduced, particularly for the downstream radiation, using a few wavepackets. However, these studies have not attempted to model the radiated coherence properties using wavepacket models, and modeling both radiation levels and coherence necessitates a more complete jet noise source model. Additionally, few, if any, studies have modeled full-scale jet noise using acoustic wavepackets, particularly for tactical jet engine noise.

C. OV ERVIEW

In this paper, a multiple-wavepacket (MWP) source model of the noise radiation from a high-performance tactical aircraft is developed using hybrid method (HM) beamforming[17] results at the jet centerline. The resultant frequency-dependent equivalent source model (ESM) predicts both the levels and temporal properties (via the coherence) of the corresponding radiation.[14, 18]

The MWP model, which is used to produce complex, extended source reconstructions over a wide frequency range, is described in Section 2 using a numerical case study to show the method's benefits and limitations. In Section 3, beamforming ESMs of tactical jet noise measurements are used as inputs to produce MWP models.

These MWP models are validated using benchmark jet noise measurements in the near and mid fields. Finally, an optimization study guides the selection of the number of wavepackets for a given frequency.

2. METHODS

In this section, a reduced-order model of beamforming-based jet noise predictions is developed. First, pressure measurements from a microphone array near an acoustic source are used as inputs to the HM beamforming algorithm, and the beamforming results produce an ESM. The beamforming-based source model is then used to create a reduced-order MWP model, which provides a simplified analytical framework and allows for extensions to other similar-typed sources. Others have attempted to model array measurements as wavepackets, including Kœnig *et al.*[4] as well as Papamoschou.[3] These studies modeled far-field measurements as a single wavepacket and included an additional component to model the residual energy. These methods were successful in modeling the far field radiation levels at the respective measurement input locations. To build upon these studies, the HM algorithm is used, which is capable of modeling source levels and coherence properties, and multiple axial wavepackets are incorporated into the source model. The MWP model is then used to predict the levels and coherence properties of the acoustic field. A numerical example is provided in which a multiple wavepacket source is used to illustrate the process and effectiveness of the beamforming and MWP model.

A. WAVEPACKET SOURCE MODEL

The HM beamforming results produce a full-order matrix solution of the original sources. However, when describing a distributed, partially correlated source, the number of elements in the beamforming source cross-spectral matrix (CSM), $\mathbf{Q}_{\mathrm{HM}}$, is s^2, where s is the number of source reconstruction locations, $\vec{r}_{i=1\ldots s}$. This number can be both large and excessive. Previous studies have shown the effectiveness of an analytical wavepacket model to efficiently predict jet noise levels within the dominant radiation lobe using very few wavepacket models, although in many cases only a single wavepacket is used.[3,4,13] A single wavepacket model produces infinite coherence in both the source and corresponding radiation—contrary to the observed finite coherence lengths in actual jet noise. Reproducing the temporal features (i.e., coherence) of the field requires a more complex model, and an analytical MWP model provides the capability to describe the finite coherence lengths present both in the source model and in the radiated field.

The MWP model is generated from the HM beamforming results, which are decomposed through an iterative process, and each analytical wavepacket is projected onto the beamforming results to extract the wavepacket's amplitude and phase contribution. Each step is summarized in Fig. 1, and an explanation of each can be found in Ref. [1].

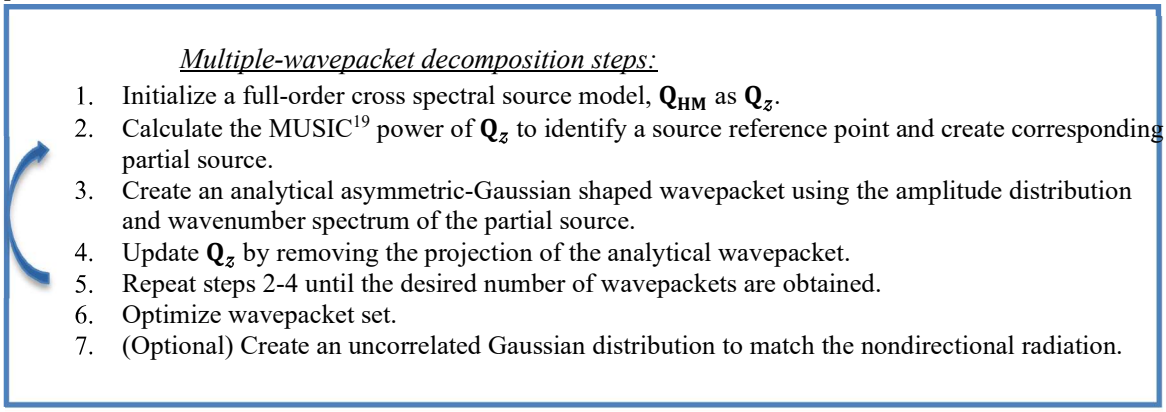

Fig. 1 Multiple wavepacket model creation process.

B. WAVEPACKET DECOMPOSITION USING A NUMERICAL SOURCE

To understand the capabilities and demonstrate the procedure of the wavepacket decomposition process, a numerical case study is presented for a single frequency. An axisymmetric source distribution consisting of six asymmetric-Gaussian wavepackets is chosen, and the magnitude and real part of the wavepackets are shown in Fig. 2(a). Each wavepacket is spatially distributed along the $+z$ axis and each contains unique parameters for various amplitudes, growth and decay rates, and peak locations. In addition, the peak wavenumber of each

wavepacket varies such that the radiation directivity ranges from 95-135°—measured from the $-z$ axis—and the directivities are assigned sequentially such that the largest directivity corresponds to the wavepacket that peaks farthest from z=0 m. In addition, the growth and decay rates and relative amplitudes of each wavepacket are varied to distinguish them.

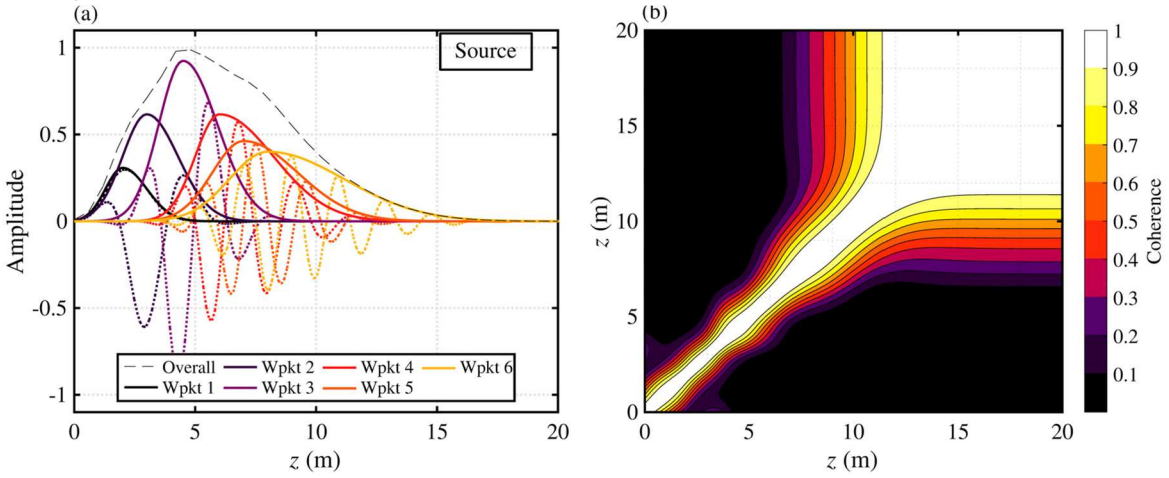

Fig. 2. (a) Numerical one-dimensional source model created using asymmetric-Gaussian- shaped wavepackets and (b) corresponding source coherence

In Fig. 2(b), the source coherence across the distribution is given, with the self-coherence shown along the diagonal and off-diagonal elements representing the coherence between two respective locations along the z axis. The source self-coherence varies as a function of position with coherence lengths that are small for $z < 9$ m, corresponding to regions where multiple wavepackets significantly overlap. Regions outside of this indicate where a single wavepacket source is the primary source.

The source distribution is aligned along the z-axis to mimic the jet noise setup shown in Fig. 3(a), with the setup assumed to lie in a free space environment. The array consists of 50 elements shown by blue dots. The array geometry mirrors the experimental setup described in Section 3A. The corresponding simulated field level calculations are shown in Fig. 3(b), and the radiation pattern is meant to simulate the jet noise directivity as seen at 250 Hz in previous studies[1].

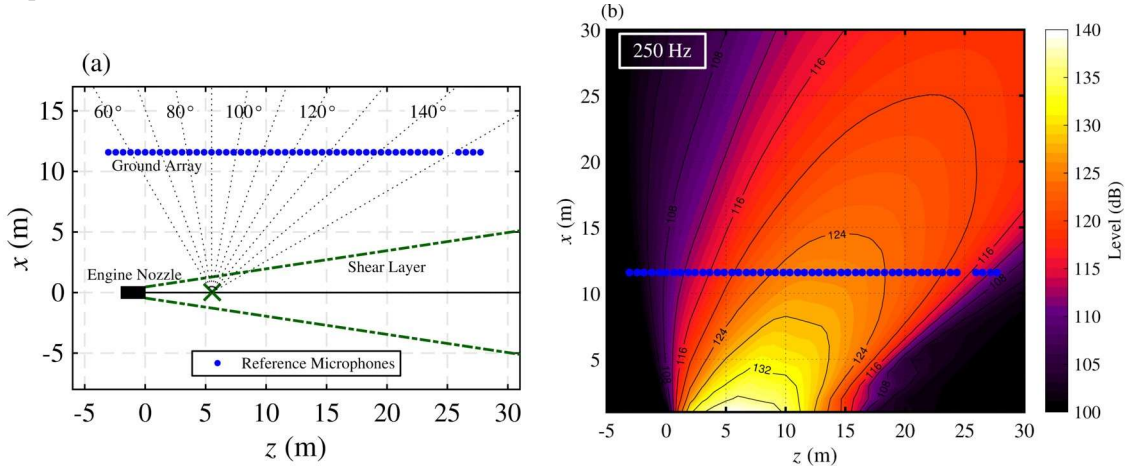

Fig. 3. (a) Numerical case geometry, with the source distributed along the z axis and (b) the corresponding simulated field levels.

The simulated array pressures are used as inputs to the HM to estimate the source CSM. The levels of the beamforming estimate (hereafter referred to as beamforming levels) are shown alongside the original overall source levels in Fig. 4. The estimated levels match the benchmark source distribution to within 1-2 dB over

locations where the levels are within 20 dB of the peak level, with the level differences growing outside of this region, particularly for $z > 12$ m. Because the wavepacket that peaks at 8 m radiates with a directivity of 135°, some of the radiation is not entirely captured by the input array, and the resultant beamforming levels are slightly underestimated. However, the large majority of the source is accurately represented and provides a strong foundation from which the MWP decomposition process can take place.

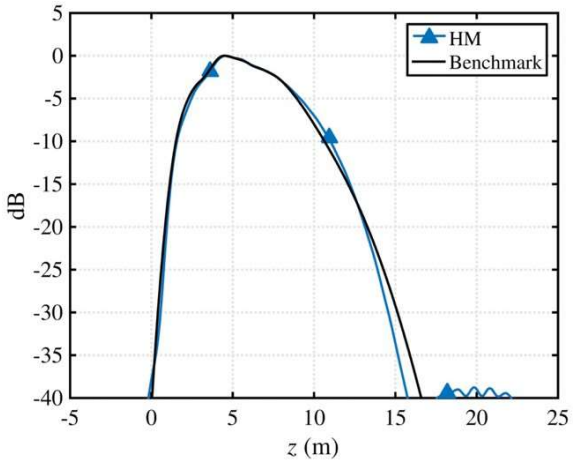

Fig. 4. Numerical source level estimate using HM beamforming, plotted with the original overall levels of the numerical source.

Next, the MWP decomposition process is performed, as shown in Fig. 1. Each analytical wavepacket is determined in an iterative process until the desired number of wavepackets is reached, which in this case is chosen as six to compare with the original wavepacket source. For each iteration, the MUSIC (Multiple Signal Classification) power[19] of the beamforming-based source CSM is calculated, and the location corresponding to the highest MUSIC power value is selected. From this location, a corresponding partial source is extracted. Having created a partial source corresponding to the highest MUSIC power location, an analytical asymmetric-Gaussian function is fit to the partial source, $\boldsymbol{q}_{\text{wpkt}}$. Generally, the analytical function represents a significant portion of the partial source, although secondary peaks in the partial source are not usually well represented. The projection of this analytical function is removed from the beamforming-based source CSM, and the process is repeated until six wavepackets are extracted.

The analytical wavepackets are optimized in a least squares process and the resultant MWP model derived from the beamforming results is shown in Fig. 5. The beamforming-based MWP model is shown in Fig. 5(a) and the numerical source is again shown in Fig. 5(b) for convenience. The combined MWP levels closely match those of the numerical source, although the individual wavepackets vary in shape and level from the original source wavepackets.

To compare the predictive capabilities of the MWP model, it is treated as an ESM and the radiated field levels are predicted using a Rayleigh integration. The estimated levels are shown in Fig. 6(a), and the error, in decibels, between the original and estimated levels is shown in Fig. 6(b). The estimated levels closely resemble those of the numerical source with errors that are generally within 1 dB of the simulated radiation levels except for the extreme upstream and downstream regions. The radiation that traverses the array at $z < 0$ m is underestimated. Because the first wavepacket in the numerical source radiates with a directivity of 95°, the radiation is underestimated in this region as the closest associated directivity in the MWP results is 109°. In addition, the levels of the radiation that propagates downstream beyond the array are significantly overestimated. This result is due to the inability of the beamforming results to accurately predict the radiation beyond the array aperture and is a common shortcoming of beamforming. Further investigation in extrapolation methods may mitigate this result[20]. However, the overall results highlight the effectiveness of the MWP model to adequately estimate the field.

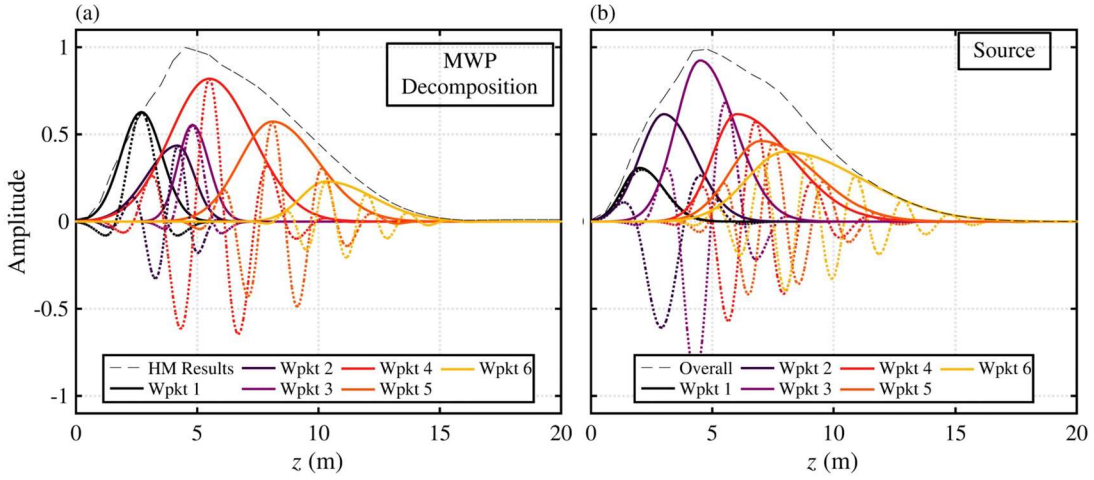

Fig. 5. (a) Beamforming results from measurements at ground-based array with corresponding wavepacket amplitude decompositions, and (b) the benchmark multiple- wavepacket source model.

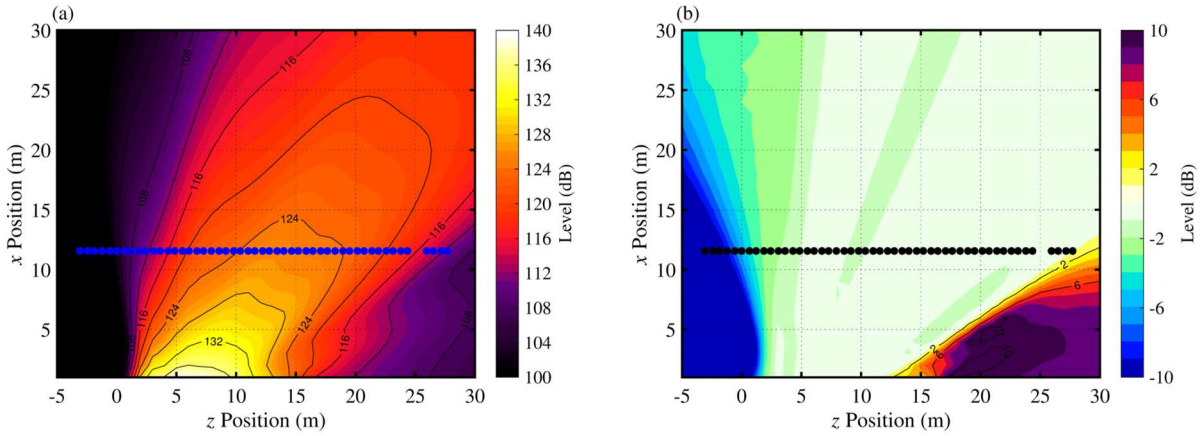

Fig. 6. (a) Predicted field levels using the MWP model and (b) the level difference, in dB, between the predicted MWP levels and simulated benchmark levels shown in Fig. 3(b).

The numerical case study highlights the capabilities and limitations of the MWP decomposition process. While the individual extracted wavepackets in the MWP model do not generally share similar properties with the numerical source in terms of their growth rate, decay rate and amplitude, they were found to have connections in terms of their center location and associated wavenumber. In particular, the directivities of the highest amplitude wavepackets were found to be within 3° of each other. In addition, the MWP model showed agreement with both the overall levels and the source coherence properties of the numerical source, and the estimated radiation levels generally agreed with the simulated levels to within 1 dB. Therefore, while many of the individual wavepacket features were not extracted, the MWP was successfully capable of representing the numerical source in terms of its cumulative properties, e.g., source level and coherence and radiation properties. In addition, the MWP model simplified the beamforming results into a reduced-order model with a similar number of partial sources as found in the numerical source.

3. EXPERIMENTAL RESULTS

The methods described in the previous section are used to analyze data taken from a full-scale turbofan engine. Measurements taken at a linear array are used as inputs to the HM beamforming algorithm to produce a full-order beamforming source model. The MWP decomposition technique is applied to the beamforming measurements in Section 3B and the MWP model is analyzed. In Section 3C, the beamforming source model

and MWP model are used to predict radiation levels at the scan array and measurement arc, and the results are compared with the benchmark measurements. In addition, the coherence measured along a linear array is compared to predictions from the beamforming and MWP models. The predicted radiation of the MWP model is analyzed to show that key radiation features are well-represented. In Section 3D, the required number of wavepackets in the MWP model is analyzed to adequately represent radiation level and coherence properties.

A. EXPERIMENT

Noise measurements were collected in the vicinity of an installed, full-scale turbofan engine at four engine conditions ranging from idle to afterburner. A planar microphone array arranged in an 18 x 5 rectangular grid pattern with 15 cm inter-element spacing was moved to multiple locations shown by triangles in Fig. 7(a). In this paper, only the microphones closest to the ground (0.38 m) are used from each planar array measurement, and they are referred to as the scan array, located 5.6 m from and parallel to the estimated shear layer. The same planar array, when placed at polar angles in the mid field between 90° and 148° (relative to the nozzle inlet) is referred to as the measurement arc. Each planar array measurement is collected at a radial distance of 23 m from the microphone array reference position, located 5.5 m downstream of the nozzle exit. The measurement arc is comprised of measurements from a single row of microphones, located at a height of 1.60 m, that are taken from each planar array measurement. A separate 50- microphone ground-based array recorded measurements simultaneously, for reference, during each planar microphone array measurement. As shown in Fig. 7(a), the ground array element spacing is 0.61 m, and the array spans 30 m. A detailed description of the experiment is found in Ref. [21].

The MIL condition data is analyzed in this paper, additional engine conditions are visited and compared in Ref. [1]. The one-third octave levels at the ground-based array are shown in Fig. 7(b) for MIL engine condition (100% engine thrust request [ETR]). At this engine condition, two primary radiation lobes are present in the ground array data, centered at $z = 12.5$ m and 400 Hz and $z = 20$ m and 125 Hz. These radiation lobes extend many meters spatially as well as across multiple third-octave measurements. A more detailed analysis of the spectral variation of the measured sound as a function of angle is provided in Ref. [22].

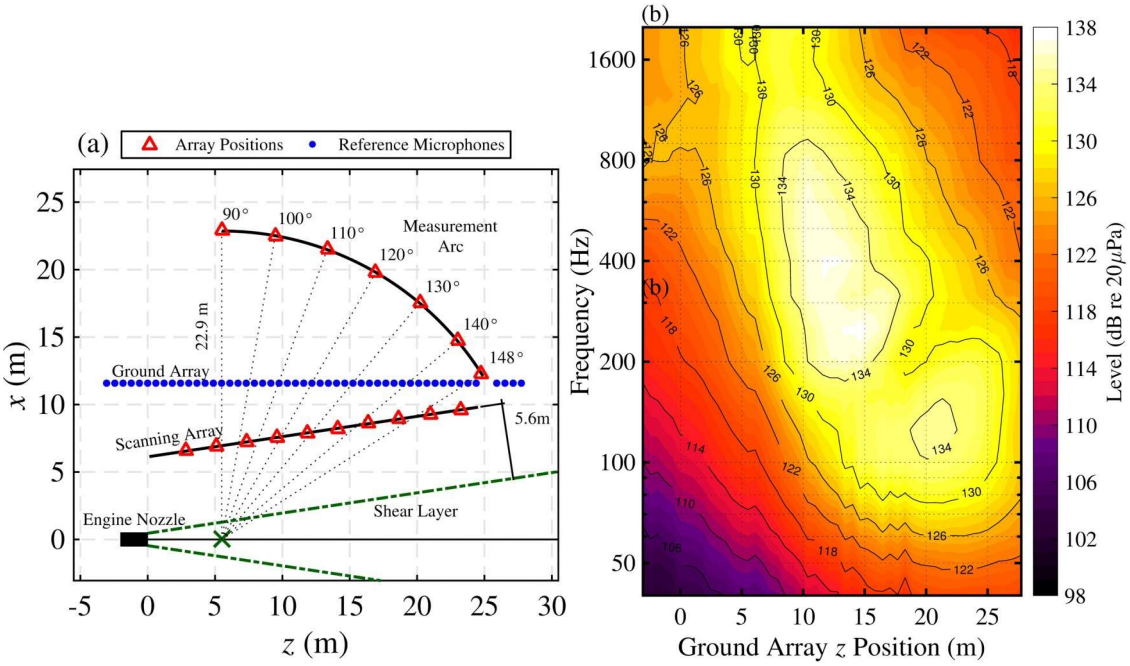

Fig. 7. (Left) Schematic of the experimental setup. Red triangle locations represent measurement positions of the 90-microphone planar array, and a ground-based array of 50 microphones are shown with blue dots. (Right) The one-third octave band levels at MIL engine condition along the ground array show evidence of a dual lobe.

B. WAVEPACKET DECOMPOSITIONS

From the equivalent beamforming-based source reconstructions[1], MWP source models are developed for six wavepackets. The decomposed MWP models are shown in Fig. 8(a-c) for 500, 200 and 100 Hz, which represent above, in, and below the supersonic transition region in the beamforming source results. The beamforming levels are shown as a solid black line, with the MWP overall level shown in a gray dotted line, and the six individual wavepackets are shown as dashed color lines. Overall, the combined level of the MWP model shows good agreement with the beamforming results, particularly at 100 Hz. However, the low-level beamforming results are not represented by the MWP model, and the individual wavepacket peaks become more evident at 500 Hz. In addition, an individual wavepacket level will exceed the overall levels in some instances. This results from the partially-coherent addition of the wavepackets and the ensuing potential for constructive and destructive interferences. While methods are implemented to produce the fewest number of wavepackets that reproduce the beamforming results, each wavepacket is finite in shape and, thus, its associated wavenumber spectrum is continuous. Therefore, some overlap occurs between the various wavepackets in the wavenumber domain and allows for interference. The individual wavepackets are therefore not orthogonal, and the degree of interference is a function of the spatial separation between the wavepackets.

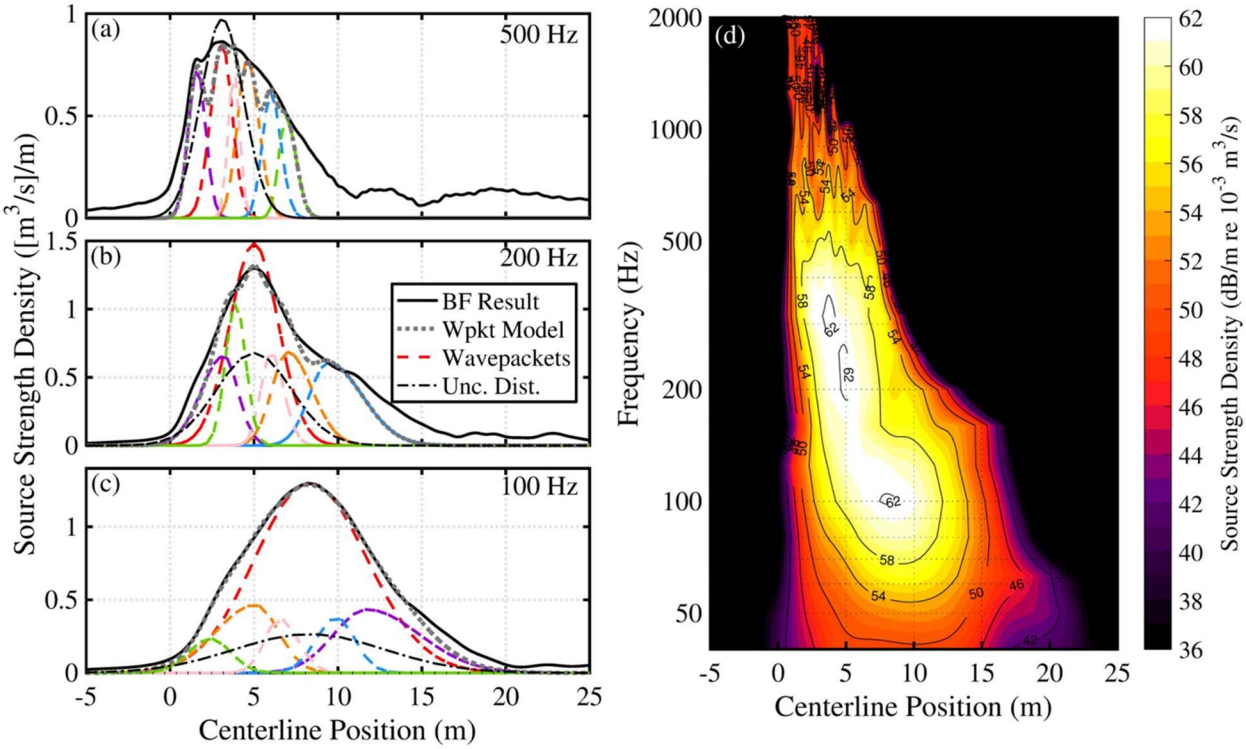

Fig. 8 Wavepacket examples at (a) 500 Hz, (b) 200 Hz, and (c) 100 Hz using six wavepackets are shown with the beamforming source strength and resultant MWP model levels. A UD is also plotted as a dash-dot line alongside each result. (d) Combined levels of the frequency dependent MWP models are shown along jet centerline.

The combined levels of the MWP models are shown in Fig. 8(d) for each of the one- third-octave, with the MWP model at each frequency corresponding to the combined levels in Fig. 8(a-c). The results share many of the salient features seen in the beamforming results[1], particularly for levels which are within the top 12 dB of the peak level for each frequency. Levels below this, however, are underpredicted by the MWP model, including regions far upstream or downstream of the main source region. This may not necessarily be problematic, as the low-level beamforming results are typically less consequential and the physical interpretation of levels below the top 12 dB may have higher errors from the HM and UPAINT[23] (Unwrapped Phase Array Interpolation) processing. In addition, results above 500 Hz become jagged, as the individual wavepacket contributions are more visible to the combined levels as seen in Fig. 8(a). These errors, produced by the reduced order of the MWP model may become large for sufficiently high frequencies, and an optimization study to determine a sufficient number of wavepackets for a given frequency is explored later.

Low-order models have been shown by Papamoschou[3] and by Koenig *et al.*[4] to be somewhat effective in describing the Mach wave radiation in far-field predictions, although they often do not entirely reproduce the radiated levels. This is solved by either increasing the order of the model (e.g., adding additional wavepackets) or by including a compensatory source. For an example of the latter, Papamoschou[3] included an additional monopole source to his single wavepacket model to boost the sideline radiation. While the effect of additional wavepackets on the source model is explored in Section 3D, an uncorrelated distribution (UD) is also applied to augment the reduced-order MWP model (see Section 5.2.1.7 of Ref. [1]). It is shown in Fig. 8(a-c) with a dash-dot line. The UD is calculated to match the levels measured along the sideline ($-2\ \text{m} \leq z \leq 5\ \text{m}$) of the input array. Due to the uncorrelated nature of this distribution, individual components that comprise the uncorrelated distribution add incoherently and, thus, produce overall levels that are less than those of the correlated distribution. A similar finding was noted by Morgan *et al.*,[24] who found that while the uncorrelated distribution levels were usually higher than the correlated source levels, they accounted for a much lower percentage of the radiated energy.

C. ESTIMATED FIELD LEVELS AND COHERENCE

An ESM allows for an efficient means to estimate and characterize the level and coherence information of the radiation field. To validate the beamforming-based ESM (hereafter referred to as beamforming model) and the computed MWP model, the estimated levels at the ground array, the scan array and the measurement arc are considered. In addition, while the input array was located at the ground, the scan array and measurement arc were at heights of 0.38 m and 1.60 m, respectively. To compensate for the additional ground-based interference patterns, an image source is modeled and propagated, together with the original source model, to predict the radiated levels at the scan array and measurement arc. The image source properties are identical to those of the original source, except that the height is mirrored about the ground plane. In addition, a test case is also included in which the uncorrelated Gaussian distribution is used to augment the wavepacket model.

Measurements at the ground array, the scan array and the measurement arc are compared to the estimated levels using the three methods at 100 Hz, 200 Hz and 500 Hz in Fig. 9. In each plot, the measurements are represented by black triangles, and the predicted levels from the beamforming source model are shown by red squares. The orange circles and purple asterisks represent the predicted levels from the MWP model and MWP model with the UD (MWP+UD model), respectively. The estimated levels from the beamforming source model and the MWP model show good agreement at all three measurement locations, within 2 dB at most locations for all frequencies, with two notable exceptions. First, the estimated levels of the MWP model along the sideline ($z < 5$ m) in many cases underestimate the measurement levels by as much as 15 dB or more. This is best seen on the measurements from the ground array, which extends up to about 4.5 m farther upstream than the scan array and about 7 m farther than the measurement arc. The addition of the uncorrelated distribution in the MWP+UD model boosts the sideline levels such that they are within measurement levels to within 2 dB throughout. Second, the predicted levels at the scan array and the measurement arc at 500 Hz are slightly larger, up to 5 dB (discounting the sideline). While the UD addition improves the sideline levels, the levels farther downstream are still slightly underpredicted as compared to the beamforming model estimates. In this case, additional wavepackets beyond the six used for the MWP model here may be necessary for improved results. The capabilities of the beamforming model and wavepacket model to estimate the field levels extend beyond the 100 Hz, 200 Hz and 500 Hz examples. This is explored in Ref. [1].

To better visualize the acoustic radiation, the beamforming model, MWP model, and MWP+UD model, having been validated in the available measurement regions shown in Fig. 9, are used to estimate the acoustic radiation near the MIL power engine on a horizontal plane at ground height for frequencies of 100 Hz, 200 Hz and 500 Hz in Fig. 10. Because the ESMs are based on ground array measurement inputs, the estimated levels are only assumed to be accurate for radiation contained within the white dashed lines. The lines coincide with the approximate aperture of the ground-based array and the jet centerline at 0 m for the upstream line and 20 m for the downstream, approximating the source region of the jet noise sources. This is only an approximate region of certainty, as the jet noise sources vary greatly in directionality with respect to source position and frequency. The field is propagated along the ground plane to better visualize the radiation without the inclusions of constructive and destructive interferences. The results show that all three models produce similar fields in the maximum radiation regions, which highlights their consistency and the capabilities of the reduced order model to capture the key characteristics of the full-order beamforming model. The primary deviation between the models lies in the sideline radiation of the MWP model, which significantly underpredicts the levels produced by the beamforming model. The MWP+UD model boosts the levels at the sideline to those like the beamforming

results. For discussion on the multi-lobed behavior seen in Fig. 10, see section 5.3 of Ref. [1] as well as Refs. [25-29].

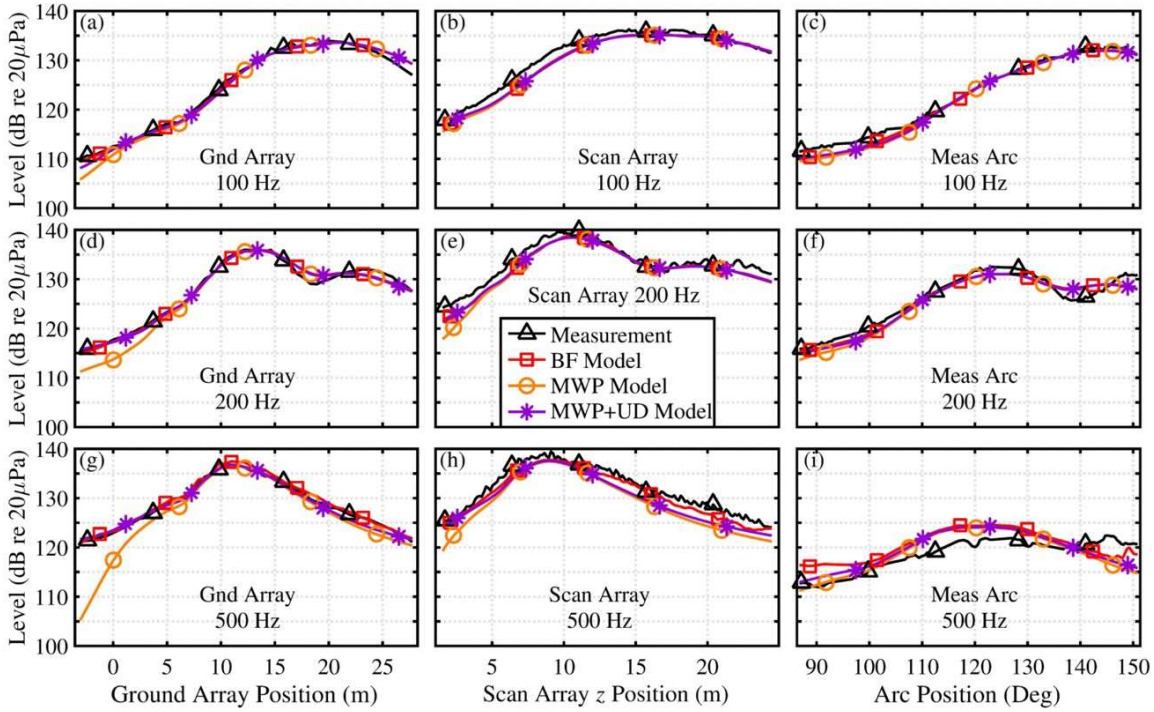

Fig. 9. Comparisons of measurements and predicted levels for (a-c) 100 Hz, (d-f) 200 Hz and (g-i) 500 Hz at (left) the ground array, (middle) the scan array, and (right) the measurement arc. The predictions are made using a beamforming model, an MWP model, and an MWP+UD model.

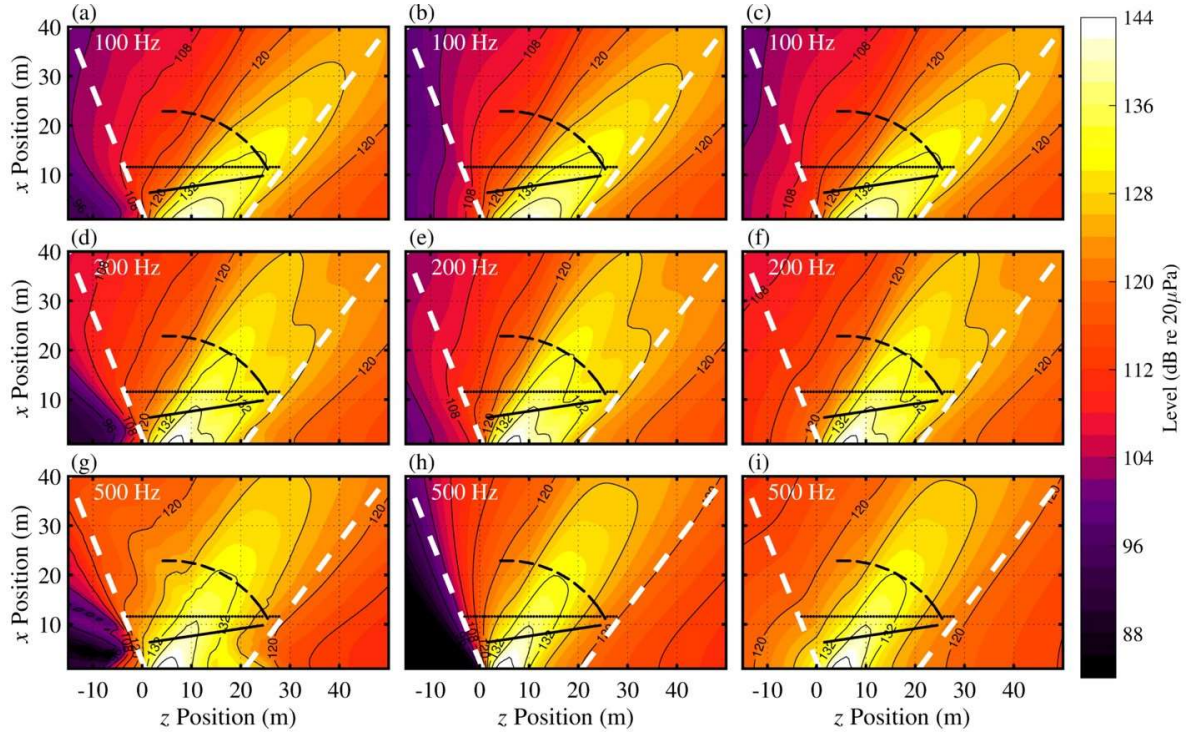

Fig. 10. Predicted levels across a horizontal plane with jet centerline on z axis. Cases for (a- c) 100 Hz, (d-f) 200 Hz, and (g-h) 500 Hz are shown using (left) a beamforming model, (middle) an MWP model, and (right) an MWP+UD model. The white-dashed lines represent the approximate aperture spanned by the ground-based array.

Whereas a single wavepacket model cannot correctly reproduce the coherence properties of the acoustic radiation and struggles to reproduce radiation at all angles,[3, 4] the MWP model produces a field with finite coherence properties. Ground array coherence calculations were used to compare the predicted coherence properties of the field using the MWP and MWP+UD source models. The results of the calculated and predicted coherence at 100, 200 and 500 Hz are shown in Fig. 11. Coherence is shown such that the self-coherence for each plot is shown along the diagonal, with a value of unity, and the off-diagonal elements represent coherence between two corresponding measurement locations along the ground array. The coherence length, L_{γ^2},values are generally largest in the region where the direction of maximum radiation traverses the ground array, at about z =10-25 m downstream. At 100 Hz, the calculated coherence lengths are greatest in the maximum radiation region [see Fig. 7(b)]. At 200 Hz, however, the multilobe radiation produces two spatial regions over which there is high coherence and a neck in the coherence map between the regions. The coherence is much lower across the array at 500 Hz, with L_{γ^2} values in the maximum radiation region not exceeding about 1 m.

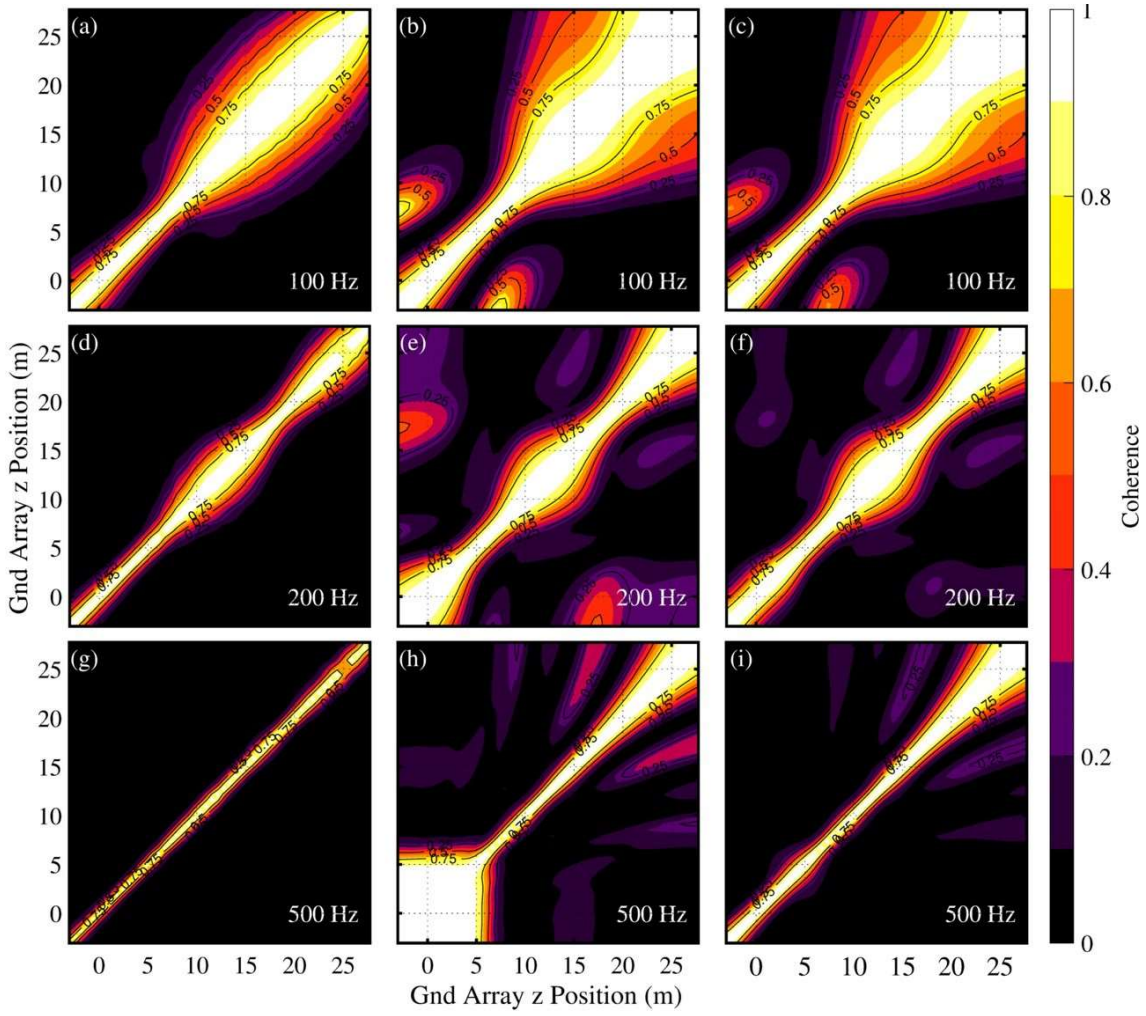

Fig. 11. Coherence values at the ground array for (a-c) 100, (d-f) 200, and (g-i) 500 Hz. The calculated coherence is shown (left), as well the predicted values using (middle) the MWP model and (right) the MWP+UD model.

The coherence is estimated at each of these frequencies using both the MWP and the MWP+UD reduced-order models. In the case of coherence estimated by the MWP model, the qualitative features found in the calculated coherence maps are present, although the coherence values are generally overestimated. For example, the coherence predictions for $z < 5$ m are greatly overestimated and bear no resemblance to the calculated coherence. In addition, coherence predictions for $z > 20$ m are also overestimated, and additional lobes in the coherence are visible at $z = 7$ m at 100 Hz and $z = 17$ m at 200 Hz that are not present in the coherence calculations from the array measurements. Thus, while the L_{γ^2} values will approximate those calculated from measurements, the additional artifacts indicate the regions where there are an insufficient number of independent

sources to better estimate the coherence. Additional wavepackets reduce the overestimation of the coherence in most regions across the measurement array, although a large number of wavepackets may be necessary to adequately reproduce the short coherence lengths to the sideline (see Ref. [30]), likely resulting from the fine-scale structure radiation identified by Neilsen *et al.*[22] using similarity spectra. The MWP+UD model incorporates the additional distributed uncorrelated source and the corresponding predicted coherence, shown in the right column of Fig. 11, improves the overestimated coherence, particularly for the sideline predictions. It also reduces the overestimation of the coherence farther downstream along the measurement array, although the result can be further improved by increasing the number of wavepackets in the MWP model. With a sufficient number of wavepackets, the inclusion of both directive wavepackets and an uncorrelated distribution allows for the accurate prediction of coherence properties both to the sideline and within the maximum radiation region where large-scale structure radiation is present.

The coherence calculations and predictions were made at the input array. Coherence predictions at additional locations will further validate the MWP capabilities. However, whereas the ground array was a synchronous measurement, measurements at the scan array and measurement arc are comprised of nonsynchronous measurements and calculating coherence values across these arrays therefore requires additional considerations and are not included in the present study.

D. OPTIMIZING THE WAVEPACKET MODEL

In the preceding analyses, six wavepackets were chosen for the MWP and MWP+UD models, regardless of frequency. This is not necessarily the optimal number of wavepackets, as fewer wavepackets might be sufficient to accurately describe the radiation, particularly at lower frequencies. In contrast, additional wavepackets may be needed for higher frequencies. To gain a sense of the required number of wavepackets for each frequency, the decibel level differences between MWP predicted and measured levels at both the scan array and the arc are averaged for each frequency. These results are averaged in a dB sense in order to equally weight the radiation levels along the array, instead of weighting the errors by the peak levels as occurs using a squared-pressure average. The errors are calculated for a variable number of included wavepackets, from one to ten, and the average errors are shown in Fig. 12(a-b) for the scan array and the measurement arc, respectively. In these plots, the horizontal axis shows the number of wavepackets used in the multiple-wavepacket model for a given frequency, and the colored contour lines provide the average error of the model. In addition, the average error of the beamforming model predicted levels is shown at the far right of each plot. As additional wavepackets are added, the errors should converge to those of the beamforming model. From the results, it is shown that by using six wavepackets, the average level errors at the scan array vary between 1-4 dB for frequencies below 400 Hz. As frequency increases, the required number of wavepackets to produce similar errors increases, and beyond 1000 Hz, errors exceeding 10 dB can result even when ten wavepackets are used. These high errors are primarily due to the increased difficulty of the MWP model to accurately estimate the sideline radiation with increasing frequency. At the measurement arc, which is located slightly farther downstream and does not include a significant portion of the sideline radiation, the errors are more consistent with frequency. Except for the errors at frequencies of 600 Hz and 2000 Hz that correspond to errors from the interference nulls, six wavepackets is sufficient to produce level estimates with average errors generally between 1-4 dB.

The predictions of the field coherence using the MWP model are also affected by the included number of wavepackets as using too few results in an overestimate of the coherence values as shown in Fig. 11. To compare the capability of the MWP model to predict the coherence properties of the field $L\gamma^2$ values are calculated at the ground array and compared to the predicted $L\gamma^2$ values using the MWP model. The $L\gamma^2$ values are calculated for every microphone reference position along the measurement array. The average error of the $L\gamma^2$ values is plotted as a function of the number of wavepackets used in the wavepacket model in Fig. 12(c). The $L\gamma^2$ values are very large (i.e., a limiting value) when only one wavepacket is used because the calculated coherence for a single source will be unity between all measurement positions. Using six wavepackets, the average $L\gamma^2$ errors range up to 2.9 m. If instead, ten wavepackets are used, the additional wavepackets improve the average $L\gamma^2$ errors, which are reduced to less than 2.0 m. In terms of wavelength, these errors therefore increase with frequency such that errors at 100 Hz correspond to about 0.5λ, while errors at 1000 Hz are large at about 4.4λ.

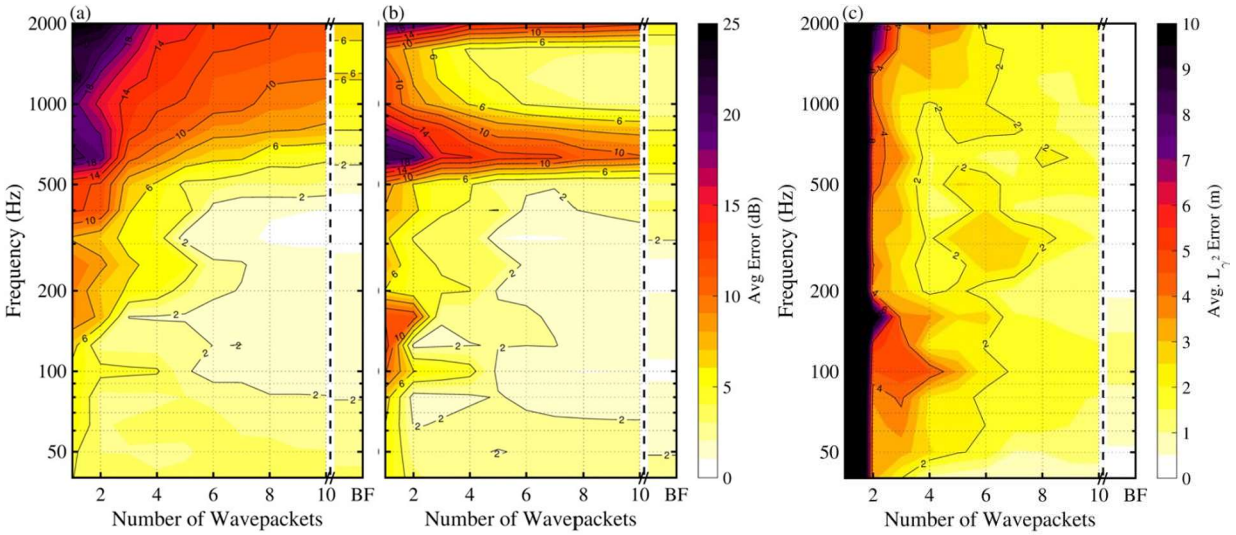

Fig. 12. Average error of MWP model predicted levels to (a) the scan array measurements and (b) the arc measurements. (c) The average error, in meters, of coherence length from wavepacket models and beamforming results to coherence calculations at the ground array. In each plot, the predicted levels and coherence length errors for each respective data of the beamforming results is plotted to the far right.

4. CONCLUSION

Multiple-wavepacket source models of the noise radiation from a high-performance tactical aircraft operating at MIL engine condition are developed using a decomposition of phased- array source reconstructions. The investigation builds on beamforming investigations that focus on source distributions as a function of frequency derived using the hybrid method (HM). The beamforming source is decomposed into a multiple-wavepacket (MWP) model consisting of six asymmetric-Gaussian-shaped wavepackets, with each having a distinct phase speed. This MWP model allows for the prediction of level-based radiation as well as coherence properties of the field where single wavepacket models fail. In addition, the MWP model can be augmented by an uncorrelated distribution (MWP+UD) to accurately predict levels where fine-scale structure radiation dominates. These models are validated using benchmark level and coherence calculations at various distances and angles in the mid field. Average errors for the MWP model vary, although they are generally within 3 dB, and errors drop further when the MWP+UD model is used. The MWP+UD improvements are due to the inability of the reduced-order MWP model to capture the sideline radiation, which would otherwise require a significant number of wavepackets. The average errors of the predicted coherence lengths in the mid field are on average less than 2.9 m using the MWP model and coherence lengths to the sideline are improved further using the MWP+UD model so that average errors drop below 2 m for the frequency range.

The MWP models are used to predict level and coherence properties across a usable aperture, defined by the measurement array used in the beamforming analysis. The results are shown alongside the predicted beamforming results, and the predicted levels using the reduced- order models show consistency with the full-order beamforming predictions.

An optimization study was also performed to determine the necessary number of wavepackets required to accurately predict the radiation and coherence properties of the field. While the addition of wavepackets reduces the error between the measured and predicted levels, these errors converge on limiting values of between 1-3 dB for frequencies below 500 Hz, although they increase with frequency due to the large sideline radiation errors. Using six wavepackets, the MWP shows level-based average predicted radiation level errors on the order of 2-3 dB for frequencies up to 500 Hz. The associated average coherence length errors fall to within about 2 m. However, when the uncorrelated distribution is included, as few as four wavepackets are sufficient to predict radiation levels to within 1-3 dB for frequencies below 500 Hz. The coherence length errors are also reduced using the MWP+UD model. For example, when four wavepackets are included in the model, the average errors fall to within less than 2 m for most frequencies below 800 Hz.

The ability of the MWP and MWP+UD models to predict the noise environment efficiently and effectively near high-performance tactical aircraft is a significant cost-reducing achievement by requiring fewer

measurements and acquisition resources. Analytical functions that produce a reduced-order source model provide a modular and scalable framework that can be used to compare with other models. In addition, the model's analytical framework allows for future work to explicitly incorporate frequency into the MWP model parameters for a more complete picture of the radiated properties. The model is also important in its ability to reproduce the more intricate features of the radiation, including the multilobe directivity patterns found in tactical aircraft measurements. Building on the successes of previous wavepacket models, the ability of the MWP model to predict coherence properties brings analytical modeling efforts closer to physical properties of the radiation. Time-domain intermittency and impulses have not been considered in the present work, and it is hypothesized that future efforts to incorporate additional physical properties of the jet noise into a reduced-order analytical framework will provide better predictive capabilities for time-domain events.[4, 8, 31] This is particularly true for future efforts to improve upon the far-field capabilities of the MWP model, particularly for large propagation distances and high frequencies where nonlinear propagation effects increase, to provide a more complete model to globally predict the radiation properties.

ACKNOWLEDGMENTS

Analysis in this paper was supported in part through the Office of Naval Research Grant N00014-14-10-494. This paper was compiled under Office of Naval Research Grant N00014-21-1-206.

Approved for public release: distribution is unlimited. 88ABW Cleared 03/29/18; 88ABW-2018-1498.

REFERENCES

[1]B. M. Harker, "Characterization of military aircraft jet noise using wavepacket analysis and other array processing methods", Brigham Young University, 2017.

[2]P. Jordan and T. Colonius, "Wave packets and turbulent jet noise," *Annual Review of Fluid Mechanics* **45**, 173-195 (2013).

[3]D. Papamoschou, "Wavepacket modeling of the jet noise source," AIAA Paper 2011-2835, 2011.

[4]M. Koenig, A. V. Cavalieri, P. Jordan, J. Delville, Y. Gervais, and D. Papamoschou, "Farfield filtering and source imaging of subsonic jet noise," *Journal of Sound and Vibration* **332**, 4067- 4088 (2013).

[5]S. C. Crow and F. Champagne, "Orderly structure in jet turbulence," *Journal of Fluid Mechanics* **48**, 547-591 (1971).

[6]A. Sinha, D. Rodríguez, G. A. Brès, and T. Colonius, "Wavepacket models for supersonic jet noise," *Journal of Fluid Mechanics* **742**, 71-95 (2014).

[7]A. Towne, A. V. Cavalieri, P. Jordan, T. Colonius, O. Schmidt, V. Jaunet, and G. A. Brès, "Acoustic resonance in the potential core of subsonic jets," *Journal of Fluid Mechanics* **825**, 1113- 1152 (2017).

[8]A. Towne, T. Colonius, P. Jordan, A. V. Cavalieri, and G. A. Brès, "Stochastic and nonlinear forcing of wavepackets in a Mach 0.9 jet," AIAA Paper 2015-2217, 2015.

[9]T. F. Brooks, W. M. Humphreys, and G. E. Plassman, "DAMAS Processing for a Phased Array Study in the NASA Langley Jet Noise Laboratory," AIAA Paper 2010-3780, 2010.

[10]R. Schlinker, S. Liljenberg, D. Polak, K. Post, C. Chipman, and A. Stern, "Supersonic Jet Noise Source Characteristics & Propagation: Engine and Model Scale," AIAA Paper 2007-3623, 2007.

[11]R. Dougherty and J. Mendoza, "Phased Array Beamforming with 100-Foot Polar Arc Microphones in a Static Engine Noise Test," AIAA Paper 2008-51, 2008.

[12]T. Suzuki and T. Colonius, "Instability waves in a subsonic round jet detected using a near-field phased microphone array," *Journal of Fluid Mechanics* **565**, 197-226 (2006).

[13]Y. Du and P. J. Morris, "Numerical simulation of the effect of a low bypass cooling stream on supersonic jet noise," AIAA Paper 2014-1402, 2014.

[14]R. Reba, S. Narayanan, and T. Colonius, "Wave-packet models for large-scale mixing noise," *International Journal of Aeroacoustics* **9**, 533-558 (2010).

[15]A. V. Cavalieri, P. Jordan, T. Colonius, and Y. Gervais, "Axisymmetric superdirectivity in subsonic jets," *Journal of Fluid Mechanics* **704**, 388-420 (2012).

[16]I. A. Maia, P. Jordan, V. Jaunet, and A. V. Cavalieri, "Two-point wavepacket modelling of jet noise," AIAA Paper 2017-3380, 2017.

[17]T. Padois, P.-A. Gauthier, and A. Berry, "Inverse problem with beamforming regularization matrix applied to sound source localization in closed wind-tunnel using microphone array," *Journal of Sound and Vibration* **333**, 6858-6868 (2014).

[18]B. M. Harker, K. L. Gee, T. B. Neilsen, A. T. Wall, and M. M. James, "Wavepacket modeling and fullscale military jet noise beamforming analyses," AIAA Paper 2016-2129, 2016.

[19]R. Schmidt, "Multiple emitter location and signal parameter estimation," *IEEE transactions on antennas and propagation* **34**, 276-280 (1986).

[20]A. T. Wall, K. L. Gee, T. B. Neilsen, R. L. McKinley, and M. M. James, "Military jet noise source imaging using multisource statistically optimized near-field acoustical holography," *The Journal of the Acoustical Society of America* **139**, 1938-1950 (2016).

[21]A. T. Wall, K. L. Gee, M. M. James, K. A. Bradley, S. A. McInerny, and T. B. Neilsen, "Near- field noise measurements of a high-performance military jet aircraft," *Noise Control Engineering Journal* **60**, 421-434 (2012).

[22]T. B. Neilsen, K. L. Gee, A. T. Wall, and M. M. James, "Similarity spectra analysis of high- performance jet aircraft noise," *Journal of the Acoustical Society of America* **133**, 2116-2125 (2013).

[23]Caleb B. Goates, Blaine M. Harker, Tracianne B. Neilsen and Kent L. Gee, "Extending the bandwidth of an acoustic beamforming array using phase unwrapping and array interpolation", *The Journal of the Acoustical Society of America,* **141**, EL407-EL412 (2017).

[24]J. Morgan, T. B. Neilsen, K. L. Gee, A. T. Wall, and M. M. James, "Simple-source model of military jet aircraft noise," *Noise Control Engineering Journal* **60**, 435-449 (2012).

[25]A. T. Wall, K. L. Gee, T. B. Neilsen, B. M. Harker, S. A. McInerny, R. C. McKinley, and M. M. James, "Investigation of multi-lobed fighter jet noise sources using acoustical holography and partial field decomposition methods," AIAA Paper 2015-2379, 2015.

[26]A. T. Wall, K. M. Leete, K. L. Gee, T. B. Neilsen, M. M. James, and R. L. McKinley, "Preliminary Investigation of Multiple Fighter Jet Noise Sources Using Acoustical Holography," AIAA Paper 2017-3520, 2017.

[27]Kevin M. Leete, Alan T. Wall, Kent L. Gee, Tracianne B. Neilsen, Michael M. James, and J. Micah Downing, "Acoustical Holography-Based Analysis of Spatiospectral Lobes in High-Performance Aircraft Jet Noise," AIAA Paper 2018-2826, 2021.

[28] Tyce Olaveson, Jacob A. Ward, Jon Paul Johnson, Kent L. Gee, and Alan T. Wall, "Analysis of Spatiospectral Lobes in Installed F404 Engine Noise Radiation," AIAA Paper 2022-3087, 2022.

[29]Logan T. Mathews, Kent L. Gee, Kevin M. Leete, and Alan T. Wall, "Acoustic Source Characterization of an Installed GE F404 Engine Using Near-field Acoustical Holography," AIAA Paper 2022-3028, 2022.

[30]B. M. Harker, T. B. Neilsen, K. L. Gee, M. M. James, and A. T. Wall, "Spatiotemporal Correlation Analysis of Jet Noise from a High-Performance Military Aircraft," AIAA Paper 2015- 2376, 2015.

[31]M. Kearney-Fischer, "A model function for jet noise events at aft angles and what it says about the statistical relationships of the events," *Journal of Sound and Vibration* **338**, 217-236 (2015).